

---

# AutoBayes: Automated Inference via Bayesian Graph Exploration for Nuisance-Robust Biosignal Analysis

---

**Andac Demir**

Department of Electrical and Computer Engineering, Northeastern University  
 360 Huntington Ave, Boston, MA 02115, USA  
[ademir@ece.neu.edu](mailto:ademir@ece.neu.edu)

**Toshiaki Koike-Akino**

Mitsubishi Electric Research Laboratories (MERL)  
 201 Broadway, Cambridge, MA 02139, USA  
[koike@merl.com](mailto:koike@merl.com)

**Ye Wang**

Mitsubishi Electric Research Laboratories (MERL)  
 201 Broadway, Cambridge, MA 02139, USA  
[yewang@merl.com](mailto:yewang@merl.com)

**Deniz Erdoğmuş**

Department of Electrical and Computer Engineering, Northeastern University  
 360 Huntington Ave, Boston, MA 02115, USA  
[erdogmus@ece.neu.edu](mailto:erdogmus@ece.neu.edu)

## Abstract

Learning data representations that capture task-related features, but are invariant to nuisance variations remains a key challenge in machine learning, in particular for biosignal processing. We introduce an automated Bayesian inference framework, called AutoBayes, that explores different graphical models linking classifier, encoder, decoder, estimator and adversary network blocks to optimize nuisance-invariant machine learning pipelines. AutoBayes also enables justifying disentangled representation, which splits the latent variable into multiple pieces to impose different relation with subject/session-variation and task labels. We benchmark the framework on a series of physiological datasets, where we have access to subject and class labels during training, and provide analysis of its capability for subject transfer learning with/without variational modeling and adversarial training. The framework can be effectively utilized in semi-supervised multi-class classification, and reconstruction tasks for datasets in different domains as well.

## 1 Introduction

The great advancement of deep learning techniques based on deep neural networks (DNN) has enabled more practical design of human-machine interfaces (HMI) through the analysis of the user's physiological data [1], such as electroencephalogram (EEG) [2], electromyogram (EMG) [3], and electrocardiogram (ECG). However, such biosignals are highly subject to variation depending on the biological states of each subject [4]. Hence, frequent calibration is often required in typical HMI systems.

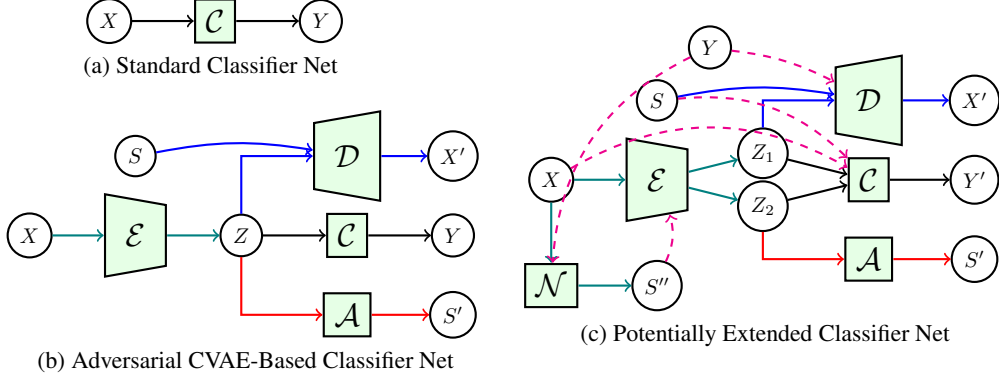


Figure 1: Inference methods to classify  $Y$  given data  $X$  under latent  $Z$  and semi-labeled nuisance  $S$ .

Toward resolving this issue, subject-invariant methods [5], employing adversarial training [6–8] with Conditional Variational AutoEncoder (A-CVAE) [9, 10] shown in Fig. 1(b), have emerged to reduce user calibration for realizing successful HMI systems. Compared to a standard DNN classifier  $C$  in Fig. 1(a), integrating additional functional blocks for encoder  $E$ , nuisance-conditional decoder  $D$ , and adversary  $A$  networks offers excellent subject-invariant performance. The DNN structure may be potentially extended with more functional blocks and more latent nodes as shown in Fig. 1(c). However, most works rely on human design and insight to determine the block connectivity and architecture of DNNs. Automation of hyperparameter and architecture exploration in the context of AutoML [11–19] can facilitate DNN design suited for subject-invariant biosignal processing. Nevertheless, without any good reasoning, most search space of link connectives will be pointless.

In this paper, we propose a systematic automation framework called AutoBayes, which searches for the best inference graph model associated to Bayesian graph model well-suited to reproduce the training datasets. The proposed method automatically formulates various different Bayesian graphs by factorizing the joint probability distribution in terms of data, class label, subject identification (ID), and inherent latent representations. Given Bayesian graphs, some meaningful inference graphs are generated through the Bayes-Ball algorithm [20] for pruning redundant links to achieve high-accuracy estimation. In order to promote robustness against nuisance parameters such as subject IDs, the explored Bayesian graphs can provide reasoning to use adversarial training with/without variational modeling and latent disentanglement. We demonstrate that AutoBayes can achieve excellent performance across various physiological datasets.

## 2 AutoBayes

At the core of our methodology is the consideration of graphical Bayesian models that capture the probabilistic relationship between random variables representing the data features  $X$ , task labels  $Y$ , nuisance variation labels  $S$ , and (potential) latent representations  $Z$ . The ultimate goal is to infer the task label  $Y$  from the measured data feature  $X$ , which is hindered by the presence of nuisance variations (e.g., inter-subject/session variations) that are (partially) labelled by  $S$ . Latent representations  $Z$  (and further denoted by  $Z_1, Z_2, \dots$ , as needed) are also optionally introduced into these models to help capture the underlying relationship between  $S, X$ , and  $Y$ .

We let  $p(y, s, z, x)$  denote the joint probability distribution underlying the biosignal datasets for the four random variables, i.e.,  $Y, S, Z$ , and  $X$ . The chain rule can yield the following factorization for a generative model from  $Y$  to  $X$  (note that at most  $4!$  factorization orders exist including useless ones):

$$p(y, s, z, x) = p(y)p(s|y)p(z|s, y)p(x|z, s, y), \quad (1)$$

which is visualized in Bayesian graph of Fig. 2(a). The probability conditioned on  $X$  can be factorized, e.g., as follows (among  $3!$  different orders of inference factorization for four-node graphs):

$$p(y, s, z|x) = \begin{cases} p(z|x)p(s|z, x)p(y|s, z, x), & \text{Z-first-inference} \\ p(s|x)p(z|s, x)p(y|z, s, x), & \text{S-first-inference} \end{cases} \quad (2)$$

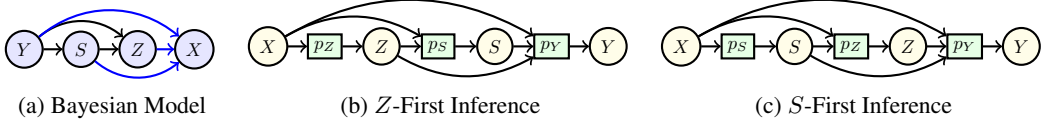


Figure 2: Fully-connected Bayesian graph and inference models for  $Z$ -first or  $S$ -first factorizations.

which are marginalized to obtain the likelihood of class  $Y$  given data  $X$ :  $p(y|x) = \mathbb{E}_{s,z} [p(y, s, z|x)]$ . The above two inference scheduling strategies in (2) are illustrated in factor graph models as in Figs. 2(b) and (c), respectively. The number of possible Bayesian graphs and inference graphs will increase rapidly when considering more nodes with multiple nuisance and latent variables.

The above graphical models in Fig. 2 does not impose any assumption of potentially inherent independency in datasets and thus most generic. However, depending on underlying independency in biosignals, we may be able to prune some edges in those graphs. For example, if the data has Markov chain of  $Y - X$  independent of  $S$  and  $Z$ , all links except one between  $X$  and  $Y$  will be unreasonable, resulting into Fig. 1(a). This implies that the most complicated inference model having high degrees of freedom does not always perform best across arbitrary datasets. It motivates us to consider an extended AutoML framework which automatically explores best pair of inference factor graph and corresponding Bayesian graph models matching datasets in addition to the hyperparameter design.

The AutoBayes begins with exploring any potential Bayesian graphs by cutting links of the full-chain graph in Fig. 2(a), imposing possible independence. We then adopt the Bayes-Ball algorithm on each hypothetical Bayesian graph to examine conditional independence over different inference strategies, e.g., full-chain  $Z$ -/ $S$ -first inference graphs in Figs. 2(b)/(c). The Bayes-Ball justifies the reasonable pruning of the links in the full-chain inference graphs Figs. 2(b)/(c), and also the potential adversary censoring when  $Z$  is independent of  $S$ . This process automatically constructs a connectivity of inference, generative, and adversary blocks with good reasoning, e.g., to construct A-CVAE classifier in Fig. 1(b) from arbitrary model of Fig. 1(c). See more detail descriptions in Appendix.

### 3 Bayesian Graph Exploration

Given biosignal measurements, we never know the true joint probability beforehand, and therefore we shall assume one of possible generative models. AutoBayes aims to explore any such potential graph models to match the measurement distributions. As the maximum possible number of graphical models is huge even for a four-node case involving  $Y$ ,  $S$ ,  $Z$  and  $X$ , we restrict our focus to a few meaningful graphs-of-interest shown in Fig. 3. Each Bayesian graph corresponds to the following assumption of the joint probability factorization ( $p(x|\dots)$  term specifies a generative model of  $X$ ):

$$p(y, s, z, x) = \begin{cases} p(y)p(s|y)p(z|\cancel{s}, y)p(x|\cancel{z}, \cancel{s}, y), & \text{Model-A} \\ p(y)p(s|\cancel{y})p(z|\cancel{s}, y)p(x|z, \cancel{s}, y), & \text{Model-B} \\ p(y)p(s|y)p(z|\cancel{s}, y)p(x|\cancel{z}, s, y), & \text{Model-C} \\ p(y)p(s|\cancel{y})p(z|s, y)p(x|z, \cancel{s}, y), & \text{Model-D} \\ p(y)p(s|\cancel{y})p(z|\cancel{s}, y)p(x|z, s, y), & \text{Model-E} \\ p(y)p(s|\cancel{y})p(z|s, \cancel{y})p(x|z, \cancel{s}, y), & \text{Model-F} \\ p(y)p(s|\cancel{y})p(z|s, y)p(x|z, s, y), & \text{Model-G} \\ p(y)p(s|\cancel{y})p(z|s, y)p(x|\cancel{z}, \cancel{s}, y), & \text{Model-H} \\ p(y)p(s|\cancel{y})p(z|s, y)p(x|\cancel{z}, s, y), & \text{Model-I} \\ p(y)p(s|\cancel{y})p(z_1|s, y)p(z_2|\cancel{z_1}, \cancel{s}, y)p(x|z_2, z_1, \cancel{s}, y), & \text{Model-J} \\ p(y)p(s|\cancel{y})p(z_1|s, y)p(z_2|z_1, \cancel{s}, y)p(x|z_2, z_1, \cancel{s}, y), & \text{Model-K} \end{cases} \quad (3)$$

where we explicitly indicate independence by slash-cancelled factors from the full-chain case in (1). Depending on the assumed Bayesian graph, the relevant inference strategy will vary as some variables may be conditionally independent, which enables pruning links in the inference factor graphs.

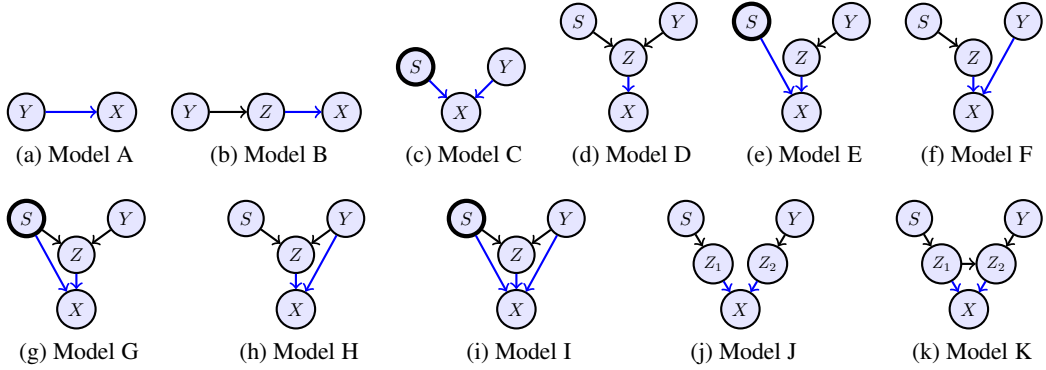


Figure 3: Example Bayesian graphs for data generative models under automatic exploration.

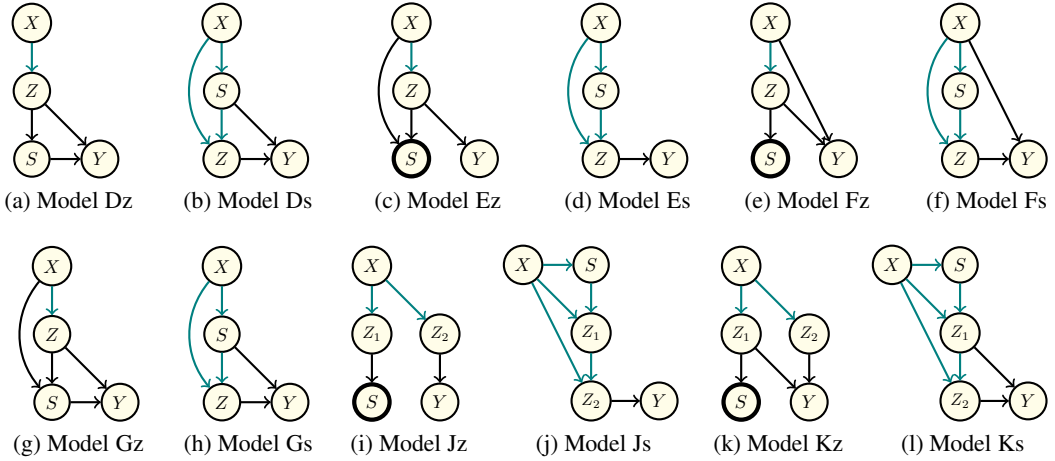


Figure 4:  $Z$ -first and  $S$ -first inference graph models relevant for generative models D–G, J, and K.

As shown in Fig. 4, the reasonable inference graph model can be automatically generated by the Bayes-Ball algorithm [20] (see Appendix) on each Bayesian graph hypothesis inherent in datasets. Specifically, the conditional probability  $p(y, s, z|x)$  can be obtained for each model as below.

**Bayesian Graph Model A (Direct Markov):** The simplest model between  $X$  and  $Y$  would be single Markov chain without any dependency of  $S$  and  $Z$ , shown in Bayesian graph of Fig. 3(a). This model puts an assumption that the biosignals are subject-invariant. For this case, there is no reason to employ complicated inference models such as A-CVAE since most factors will be independent as  $p(y, s, z|x) = p(z|x)p(s|z, x)p(y|s, z, x)$ . We hence should use a standard classification method, as in Fig. 1(a), to infer  $Y$  given  $X$ , based on the inference model  $p(y|x)$  without involving  $S$  and  $Z$ .

**Bayesian Graph Model B (Markov Latent):** Assuming a latent  $Z$  can work in a Markov chain of  $Y - Z - X$  shown in Fig. 3(b), we obtain a simple inference model:  $p(y, s, z|x) = p(z|x)p(s|z, x)p(y|s, z, x)$ . Note that this model assumes independence between  $Z$  and  $S$ , and thus adversarial censoring [6–8] can make it more robust against nuisance.

**Bayesian Graph Model C (Subject-Dependent):** We may model the case when the data  $X$  directly depends on subject  $S$  and task  $Y$ , shown in Fig. 3(c). For this case, we may consider the corresponding inference models due to the Bayes-Ball:

$$p(y, s, z|x) = \begin{cases} p(s|x)p(z|s, x)p(y|s, z, x), & \text{Model-Cs} \\ p(y|x)p(s|y, x)p(z|y, x) & \text{Model-Cy} \end{cases} \quad (4)$$

Note that this model does not depend on  $Z$ , and thus  $Z$ -first inference strategy reduces to  $S$ -first model. As a reference, we here consider additional  $Y$ -first inference strategy to evaluate the difference.

**Bayesian Graph Model D (Latent Summary):** Another graphical model is shown in Fig. 3(d), where a latent space bridges all other random variables. Bayes-Ball yields the following models:

$$p(y, s, z|x) = \begin{cases} p(z|x)p(s|z, \not{x})p(y|s, z, \not{x}), & \text{Model-Dz} \\ p(s|x)p(z|s, x)p(y|z, s, \not{x}), & \text{Model-Ds} \end{cases} \quad (5)$$

whose graphical models are depicted in Figs. 4(a) and (b), respectively.

**Bayesian Graph Model E (Task-Summary Latent):** Another graphical model involving latent variables is shown in Fig. 3(e), where a latent space only summarizes  $Y$ . Bayes-Ball yields the following inference models:

$$p(y, s, z|x) = \begin{cases} p(z|x)p(s|z, x)p(y|z, \not{s}, \not{x}), & \text{Model-Ez} \\ p(s|x)p(z|s, x)p(y|\not{s}, z, \not{x}), & \text{Model-Es} \end{cases} \quad (6)$$

which are illustrated in Figs. 4(c) and (d). Note that the generative model E has no marginal dependency between  $Z$  and  $S$ , which provides the reason to use adversarial censoring to suppress nuisance information  $S$  in the latent space  $Z$ . In addition, because the generative model of  $X$  is dependent on both  $Z$  and  $S$ , it is justified to employ the A-CVAE classifier shown in Fig. 1(b).

**Bayesian Graph Model F (Subject-Summary Latent):** Consider Fig. 3(f), where a latent variable summarizes subject information  $S$ . The Bayes-Ball provides the inference graphs shown in Figs. 4(e) and (f), which respectively correspond to:

$$p(y, s, z|x) = \begin{cases} p(z|x)p(s|z, \not{x})p(y|\not{s}, x, z), & \text{Model-Fz} \\ p(s|x)p(z|s, x)p(y|x, \not{s}, z), & \text{Model-Fs} \end{cases} \quad (7)$$

**Bayesian Graph Model G:** Letting the joint distribution follow the model G in Fig. 3(g), we obtain the following inference models via the Bayes-Ball:

$$p(y, s, z|x) = \begin{cases} p(z|x)p(s|z, x)p(y|s, z, \not{x}), & \text{Model-Gz} \\ p(s|x)p(z|s, x)p(y|z, s, \not{x}), & \text{Model-Gs} \end{cases} \quad (8)$$

whose graphical models are described in Figs. 4(g) and (h). Note that the inference model Gs in Fig. 4(h) is identical to the inference model Ds in Fig. 4(b). Although the inference graphs Gs and Ds are identical, the generative model of  $X$  is different as shown in Figs. 3(g) and (d). Specifically, VAE decoder for the model G should feed  $S$  along with variational latent space  $Z$ , and thus using CVAE is justified for the model G but D. This difference of the generative models can potentially make a different impact on the performance of inference despite the inference graph alone is identical.

**Bayesian Graph Models H and I:** Both the generative models H and I shown in Figs. 3(h) and (i) have the fully-connected inference strategies as given in (2), whose graphs are shown in Figs. 2(b) and (c), respectively, since no useful conditional independency can be found with the Bayes-Ball. Analogous to the relation of models Ds and Gs, the inference graph can be identical for Bayesian graphs H and I, whereas the generative model of  $X$  is different as shown in Figs. 3(h) and (i).

**Bayesian Graph Model J (Disentangled Latent):** We can also consider multiple latent vectors to generalize the Bayesian graph with more vertices. We here focus on two such examples of graph models with two-latent spaces as shown in Figs. 3(j) and (k). Those models are identical class of the model D, except that a single latent  $Z$  is disentangled into two parts  $Z_1$  and  $Z_2$ , respectively associated with  $S$  and  $Y$ . Given the Bayesian graph of Fig. 3(j), the Bayes-Ball yields some inference strategies including the following two models:

$$p(y, s, z_1, z_2|x) = \begin{cases} p(z_1, z_2|x)p(s|z_1, \not{z_2}, \not{x})p(y|\not{s}, \not{z_1}, z_2, \not{x}), & \text{Model-Jz} \\ p(s|x)p(z_1|s, x)p(z_2|\not{s}, z_1, x)p(y|\not{s}, \not{z_1}, z_2, \not{x}), & \text{Model-Js} \end{cases} \quad (9)$$

which are shown in Figs. 4(i) and (j). Note that  $Z_2$  is marginally independent of the nuisance variable  $S$ , which encourages the use of adversarial training to be robust against subject/session variations.

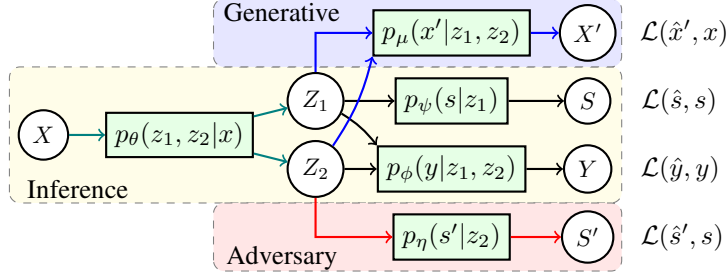


Figure 5: Overall network structure for pairing generative model K and inference model Kz.

**Bayesian Graph Model K (Conditionally Disentangled Latent):** Another modified model in Fig. 3(k) linking  $Z_1$  and  $Z_2$  yields the following inference models:

$$p(y, s, z_1, z_2|x) = \begin{cases} p(z_1, z_2|x)p(s|z_1, z_2, \mathbf{x})p(y|s, z_1, z_2, \mathbf{x}), & \text{Model-Kz} \\ p(s|x)p(z_1|s, x)p(z_2|s, z_1, x)p(y|s, z_1, z_2, \mathbf{x}), & \text{Model-Ks} \end{cases} \quad (10)$$

as shown in Figs. 4(k) and (l). The major difference from the model J lies in the fact that the inference graph should use  $Z_1$  along with  $Z_2$  to infer  $Y$ .

As described in the above examples, AutoBayes explores different Bayesian graphs Fig. 3 by assuming independent factors in (3) to generate a few inference graphs Fig. 4 through the Bayes-Ball algorithm to prune links. Given a pair of generative graph and inference graph, the corresponding DNN structures will be trained. For example of the generative graph model K in Fig. 3(k), one relevant inference graph Kz in Fig. 4(k) will result in the overall network structure as shown in Fig. 5, where adversary network is attached as  $Z_2$  is (conditionally) independent of  $S$ . Each factor block is realized by a DNN, e.g.,  $p_\theta(z_1, z_2|x)$  is a DNN parameterized by  $\theta$ , and whole networks except adversary network are optimized to minimize corresponding loss functions including  $\mathcal{L}(\hat{y}, y)$  as follows:

$$(\theta, \psi, \eta, \mu) = \arg \min_{\theta, \psi, \eta, \mu} \mathbb{E} [\mathcal{L}(\hat{y}, y) + \lambda_s \mathcal{L}(\hat{s}, s) + \lambda_x \mathcal{L}(\hat{x}', x) + \lambda_z \mathbb{KL}(z_1, z_2) - \lambda_a \mathcal{L}(\hat{s}', s)], \quad (11)$$

$$(z_1, z_2) = p_\theta(x), \quad \hat{y} = p_\psi(z_1, z_2), \quad \hat{s} = p_\phi(z_1), \quad \hat{x}' = p_\mu(z_1), \quad \hat{s}' = p_\eta(z_1, z_2), \quad (12)$$

where  $\lambda_*$  denotes a regularization coefficient,  $\mathbb{KL}$  is the Kullback–Leibler divergence, and the adversary network  $p_\eta(s'|z_2)$  is trained to minimize  $\mathcal{L}(\hat{s}', s)$  in an alternating fashion (see Appendix).

## 4 Experimental Evaluation

### 4.1 Datasets

We experimentally demonstrate the performance of AutoBayes for publicly available physiological datasets as well as a benchmark MNIST as follows. See more detail information in Appendix.

- **QMNST:** A benchmark hand-written digit image MNIST dataset with extended label information including a writer ID number [21]. There are  $|S| = 539$  writers for classifying  $|Y| = 10$  digits from grayscale  $28 \times 28$  pixel images over 60,000 training samples.
- **Stress:** A physiological dataset considering neurological stress level [22].  $|Y| = 4$  discrete stress states from  $|S| = 20$  subjects. The data were recorded with  $C = 7$  sensors including heart rates, electrodermal activity, temperature, and arterial oxygen level, for 300 samples.
- **RSVP:** An EEG data for rapid serial visual presentation (RSVP) drowsiness [23].  $|S| = 10$  subjects at three sessions for 41,400 epochs of  $C = 16$  channels for  $T = 128$  samples.  $|Y| = 4$  labels for emotion elicitation, resting-state, or motor imagery/execution task.
- **MI:** The PhysioNet EEG Motor Imagery (MI) dataset [24]. The dataset consists of  $T = 480$  samples of  $C = 64$  channels data for  $|S| = 106$  subjects.  $|Y| = 4$ -class MI task for 90 trials.
- **ErrP:** An error-related potential (ErrP) of EEG dataset [25]. The data consists of  $|S| = 16$  subjects participating in spelling task, recorded from  $C = 56$  channels over  $T = 250$  samples for 340 trials.  $|Y| = 2$  binary labels for erroneous or correct feedback.

Table 1: Performance of datasets: the reconstruction loss, the scores of nuisance classification and task classification in variational/non-variational and adversarial/non-adversarial setting.

Dataset	Method	Reconstruction Loss (dB)		Nuisance Classification (%)		Task Classification (%)	
		Non-Variational	Variational	Non-Variational	Variational	Non-Variational	Variational
QMnist	Model A	−43.4	—	—	—	97.7	—
	Model B	−62.0	−41.4	—	—	89.3	10.5
	Model Cs	−45.5	—	7.0	—	97.5	—
	Model Cy	−45.3	—	8.2	—	97.5	—
	Model Ds	−61.1	−41.4	6.8	7.4	92.9	90.7
	Model Dz	−61.2	−41.4	4.1	0.2	88.5	9.8
	Model Es	−60.6	−41.5	6.9	7.0	89.9	87.8
	Model Ez	−60.0	−58.6	7.3	7.0	88.3	86.5
	Model Fs	−60.9	−43.3	6.7	6.5	97.8	97.8
	Model Fz	−61.6	−43.3	3.5	3.1	98.1	97.9
	Model Gs	−59.9	−53.0	6.5	7.1	91.0	90.5
	Model Gz	−60.7	−58.4	7.6	7.3	91.2	89.3
	Model H	−60.7	−43.4	8.5	7.2	97.4	97.6
	Model I	−63.2	−45.2	8.1	6.6	97.8	97.3
Stress	Model Js	−67.1	−39.2	6.8	6.8	89.9	86.9
	Model Jz	−66.2	−58.1	6.8	6.9	90.0	87.0
	Model Ks	−68.4	−57.3	6.9	6.9	96.9	96.2
	Model Kz	−65.5	−54.5	4.4	4.2	98.6	97.2
	Model A	−50.8	—	—	—	87.6	—
	Model B	−79.2	−48.4	—	—	86.7	30.9
	Model Cs	−61.4	—	78.3	—	89.7	—
	Model Cy	−61.5	—	78.9	—	88.5	—
	Model Ds	−73.2	−48.4	79.4	79.4	87.1	84.3
	Model Dz	−80.9	−48.3	46.9	4.8	83.3	30.7
	Model Es	−76.5	−72.0	79.2	80.4	69.3	59.4
	Model Ez	−80.0	−48.3	81.6	62.6	84.8	30.0
	Model Fs	−72.8	−50.8	79.8	79.5	90.6	77.6
	Model Fz	−80.0	−48.3	46.0	6.9	85.7	75.3
	Model Gs	−74.0	−71.4	79.8	76.7	88.0	81.7
	Model Gz	−80.9	−48.3	80.5	76.1	88.8	87.5
	Model H	−79.2	−50.9	81.4	79.9	88.2	83.6
	Model I	−80.7	−61.2	88.5	80.6	91.0	88.2
RSVP	Model Js	−66.7	−64.7	84.5	87.7	77.4	83.6
	Model Jz	−83.1	−48.2	43.8	45.0	79.0	74.4
	Model Ks	−83.1	−65.0	79.3	79.3	64.6	78.5
	Model Kz	−83.1	−40.0	42.4	42.0	85.5	92.6
	Model A	−38.9	—	—	—	92.6	—
	Model B	−45.3	−38.5	—	—	93.2	92.9
	Model Cs	−39.2	—	91.8	—	93.0	—
	Model Cy	−39.2	—	91.4	—	93.0	—
	Model Ds	−45.3	−38.9	91.3	91.7	93.1	93.0
	Model Dz	−45.3	−38.9	38.5	12.1	93.2	92.9
	Model Es	−45.3	−38.9	91.6	91.6	92.7	93.2
	Model Ez	−45.5	−39.3	90.5	92.1	92.9	93.1
	Model Fs	−45.8	−39.3	92.9	92.2	92.2	93.1
	Model Fz	−65.4	−40.0	39.4	10.1	92.7	91.9
	Model Gs	−45.8	−39.3	91.3	90.9	93.1	93.0
	Model Gz	−45.4	−39.2	91.6	91.7	93.0	92.5
	Model H	−45.7	−38.9	91.5	91.8	92.7	93.1
	Model I	−45.3	−38.9	51.0	51.5	93.5	93.9
	Model Js	−48.8	−39.8	91.6	91.3	92.9	93.0
	Model Jz	−49.0	−39.7	40.9	42.2	93.1	92.9
	Model Ks	−48.9	−39.9	92.6	92.0	92.8	93.0
	Model Kz	−48.9	−39.9	34.5	43.6	92.8	93.5

## 4.2 Model Implementation

All models were trained with a minibatch size of 64 using Adam optimizer with an initial learning rate of 0.001. The learning rate is halved whenever the validation loss plateaus. A compact convolutional neural network (CNN) with 4 layers is employed as an encoder network  $\mathcal{E}$  to extract features from  $C \times T$  multi-channel biomedical data. First 3 layers have 1-dimensional (D) temporal

Table 1: Performance of datasets (continued)

Dataset	Method	Reconstruction Loss (dB)		Nuisance Classification (%)		Task Classification (%)	
		Non-Variational	Variational	Non-Variational	Variational	Non-Variational	Variational
MI	Model A	−40.7	—	—	—	51.3	—
	Model B	−45.9	−42.5	—	—	52.5	40.4
	Model Cs	−40.0	—	84.3	—	54.4	—
	Model Cy	−40.8	—	80.7	—	52.2	—
	Model Ds	−45.7	−41.5	84.8	83.4	54.7	30.7
	Model Dz	−52.8	−39.4	74.4	92.1	68.6	93.1
	Model Es	−45.7	−40.0	82.3	83.5	51.7	25.5
	Model Ez	−45.8	−42.5	4.8	1.6	47.4	52.0
	Model Fs	−45.7	−40.0	82.6	83.5	51.9	45.5
	Model Fz	−45.8	−42.5	4.8	4.6	47.4	51.4
	Model Gs	−45.7	−40.3	82.9	85.4	47.4	35.6
	Model Gz	−45.7	−42.5	78.0	83.4	46.0	34.0
	Model H	−45.9	−42.5	78.2	73.8	50.3	49.7
	Model I	−42.5	−45.5	84.0	85.0	53.6	49.2
	Model Js	−47.0	−40.0	85.7	51.0	42.3	38.1
	Model Jz	−47.1	−40.0	45.3	6.6	35.4	26.6
	Model Ks	−47.6	−36.5	83.1	48.0	48.1	48.0
	Model Kz	−47.0	−36.5	6.4	1.1	51.3	45.2
ErrP	Model A	−37.7	—	—	—	69.2	—
	Model B	−51.7	−38.5	—	—	73.9	71.6
	Model Cs	−36.9	—	98.0	—	62.5	—
	Model Cy	−36.0	—	99.8	—	66.2	—
	Model Ds	−52.5	−37.1	99.5	99.4	67.3	70.3
	Model Dz	−52.7	−51.6	68.8	59.5	70.6	68.1
	Model Es	−51.4	−52.3	99.4	99.2	67.9	70.6
	Model Ez	−51.7	−43.4	99.6	98.7	68.6	70.7
	Model Fs	−51.8	−36.6	99.0	92.1	71.0	62.4
	Model Fz	−52.5	−38.1	40.0	40.0	71.2	71.8
	Model Gs	−52.8	−42.0	99.5	99.3	71.0	71.0
	Model Gz	−51.1	−43.6	99.4	99.3	71.5	68.3
	Model H	−52.8	−37.0	99.4	99.5	70.1	71.0
	Model I	−51.8	−36.4	99.1	98.3	70.1	70.3
	Model Js	−61.0	−37.0	99.1	99.3	68.6	56.4
	Model Jz	−60.6	−50.7	39.1	45.3	68.4	70.7
	Model Ks	−51.8	−51.7	99.3	99.2	68.1	67.8
	Model Kz	−61.5	−50.2	43.5	46.3	70.9	68.2

convolution kernels to exploit long, medium and short term temporal dependencies. Each temporal convolution is followed by batch normalization and rectified linear unit (ReLU) activation. Final convolution layer is a 1D spatial convolution across all the channels. The AutoBayes chooses either a deterministic latent encoder or variational latent encoder under Gaussian prior. The original data is reconstructed by a decoder network  $\mathcal{D}$  that applies 1D spatial and temporal transposed convolutions of the same kernel resolutions. Data is split into train (70%) and validation (30%). All methods are without data augmentation and initialized with data normalization. For models where adversarial training is available, the regularization parameter  $\lambda_a$  is set to 0.01. See Appendix for more details.

Note that AutoBayes can be readily integrated with AutoML to optimize any hyperparameters of individual DNN blocks. Nevertheless, as our primary objective is to show a proof-of-concept benefit from solely graphical model exploration of AutoBayes, we leave more rigorous analysis to optimize DNN parameters such as network depths, widths, activation, augmentation etc. as a future work.

### 4.3 Results

The results in Table 1 suggest that the best inference strategy highly depends on datasets. Specifically, the best model at one dataset does not perform best for different datasets; e.g., the model Kz was best for Stress dataset, while the simple model B was best for ErrP dataset. It suggests that we shall consider different inference strategies for each target dataset adaptively. The AutoBayes provides such an adaptive framework. In addition, a huge performance gap between the best and worst models was observed for each dataset. For example, the task accuracy of 93.1% was achieved with model Dz for MI dataset, whereas the model Es offers 25.5%. This implies that we may have

a potential risk that one particular model cannot achieve good performance if we do not explore different models. Also note that reconstruction loss may not be a good indicator to select the graph model. How to efficiently explore potential graphs will remain as a future work.

## 5 Conclusion and Future Work

We proposed a new concept called AutoBayes which explores various different Bayesian graph models to facilitate searching for the best inference strategy, suited for nuisance-robust HMI systems. With the Bayes-Ball algorithm, our method can automatically construct reasonable link connections among classifier, encoder, decoder, nuisance estimator and adversary DNN blocks. As a proof-of-concept analysis, we demonstrated the benefit of AutoBayes for various neuro-/physio-logical datasets. We observed a huge performance gap between the best and worst graph models, implying that the use of one deterministic model without graph exploration can potentially suffer a poor classification result. In addition, the best model at one physiological dataset does not always perform best for different data, that encourages us to use AutoBayes for adaptive model generation given target datasets. We are extending the AutoBayes framework to integrate AutoML to optimize hyperparameters of each DNN block. How to handle the exponentially growing search space of possible Bayesian graphs along with the number of random variables remains a challenging future work.

## Broader Impact

Our work aims to automate the discovery and exploitation of graphical Bayesian models with the aim of mitigating nuisance variations. An ultimate application that we envision is the improvement of HMI systems to be more robust to inter-subject variations and require less calibration. Such improvements could benefit some physically disadvantaged populations that rely more on mechanical assistance. Since this work is still in the fundamental research stage, we believe there are no immediate ethical or societal concerns.

## References

- [1] Oliver Faust, Yuki Hagiwara, Tan Jen Hong, Oh Shu Lih, and U Rajendra Acharya. Deep learning for healthcare applications based on physiological signals: A review. *Computer methods and programs in biomedicine*, 161:1–13, 2018.
- [2] Vernon J Lawhern, Amelia J Solon, Nicholas R Waytowich, Stephen M Gordon, Chou P Hung, and Brent J Lance. EEGNet: a compact convolutional neural network for EEG-based brain-computer interfaces. *Journal of neural engineering*, 15(5):056013, 2018.
- [3] Manfredo Atzori, Matteo Cognolato, and Henning Müller. Deep learning with convolutional neural networks applied to electromyography data: A resource for the classification of movements for prosthetic hands. *Frontiers in neurorobotics*, 10:9, 2016.
- [4] Christoforos Christoforou, Robert M Haralick, Paul Sajda, and Lucas C Parra. The bilinear brain: towards subject-invariant analysis. In *2010 4th International Symposium on Communications, Control and Signal Processing (ISCCSP)*, pages 1–6. IEEE, 2010.
- [5] Ozan Özdenizci, Ye Wang, Toshiaki Koike-Akino, and Deniz Erdoğmuş. Transfer learning in brain-computer interfaces with adversarial variational autoencoders. In *2019 9th International IEEE/EMBS Conference on Neural Engineering (NER)*, pages 207–210. IEEE, 2019.
- [6] Alireza Makhzani, Jonathon Shlens, Navdeep Jaitly, Ian Goodfellow, and Brendan Frey. Adversarial autoencoders. *arXiv preprint arXiv:1511.05644*, 2015.
- [7] Guillaume Lample, Neil Zeghidour, Nicolas Usunier, Antoine Bordes, Ludovic Denoyer, and Marc’Aurelio Ranzato. Fader networks: Manipulating images by sliding attributes. In *Advances in Neural Information Processing Systems*, pages 5967–5976, 2017.
- [8] Antonia Creswell, Anil A Bharath, and Biswa Sengupta. Conditional autoencoders with adversarial information factorization. *arXiv preprint arXiv:1711.05175*, 2017.
- [9] Christos Louizos, Kevin Swersky, Yujia Li, Max Welling, and Richard Zemel. The variational fair autoencoder. *arXiv preprint arXiv:1511.00830*, 2015.

[10] Kihyuk Sohn, Honglak Lee, and Xinchen Yan. Learning structured output representation using deep conditional generative models. In *Advances in neural information processing systems*, pages 3483–3491, 2015.

[11] Anubhav Ashok, Nicholas Rhinehart, Fares Beainy, and Kris M Kitani. N2N learning: Network to network compression via policy gradient reinforcement learning. *arXiv preprint arXiv:1709.06030*, 2017.

[12] Andrew Brock, Theodore Lim, James M Ritchie, and Nick Weston. Smash: one-shot model architecture search through hypernetworks. *arXiv preprint arXiv:1708.05344*, 2017.

[13] Han Cai, Tianyao Chen, Weinan Zhang, Yong Yu, and Jun Wang. Reinforcement learning for architecture search by network transformation. *arXiv preprint arXiv:1707.04873*, 2017.

[14] Yihui He, Ji Lin, Zhijian Liu, Hanrui Wang, Li-Jia Li, and Song Han. AMC: AutoML for model compression and acceleration on mobile devices. In *Proceedings of the European Conference on Computer Vision (ECCV)*, pages 784–800, 2018.

[15] Risto Miikkulainen, Jason Liang, Elliot Meyerson, Aditya Rawal, Daniel Fink, Olivier Francon, Bala Raju, Hormoz Shahrzad, Arshak Navruzyan, Nigel Duffy, et al. Evolving deep neural networks. In *Artificial Intelligence in the Age of Neural Networks and Brain Computing*, pages 293–312. Elsevier, 2019.

[16] Esteban Real, Sherry Moore, Andrew Selle, Saurabh Saxena, Yutaka Leon Suematsu, Jie Tan, Quoc V Le, and Alexey Kurakin. Large-scale evolution of image classifiers. In *Proceedings of the 34th International Conference on Machine Learning-Volume 70*, pages 2902–2911. JMLR.org, 2017.

[17] Esteban Real, Chen Liang, David R So, and Quoc V Le. AutoML-Zero: Evolving machine learning algorithms from scratch. *arXiv preprint arXiv:2003.03384*, 2020.

[18] Kenneth O Stanley and Risto Miikkulainen. Evolving neural networks through augmenting topologies. *Evolutionary computation*, 10(2):99–127, 2002.

[19] Barret Zoph, Vijay Vasudevan, Jonathon Shlens, and Quoc V Le. Learning transferable architectures for scalable image recognition. In *Proceedings of the IEEE conference on computer vision and pattern recognition*, pages 8697–8710, 2018.

[20] Ross D Shachter. Bayes-Ball: The rational pastime (for determining irrelevance and requisite information in belief networks and influence diagrams). *arXiv preprint arXiv:1301.7412*, 2013.

[21] Chhavi Yadav and Léon Bottou. Cold case: The lost MNIST digits. In *Advances in Neural Information Processing Systems 32*. Curran Associates, Inc., 2019.

[22] Javad Birjandtalab, Diana Cogan, Maziyar Baran Pouyan, and Mehrdad Nourani. A non-EEG biosignals dataset for assessment and visualization of neurological status. In *2016 IEEE International Workshop on Signal Processing Systems (SiPS)*, pages 110–114. IEEE, 2016.

[23] Umut Orhan, Kenneth E Hild, Deniz Erdogmus, Brian Roark, Barry Oken, and Melanie Fried-Oken. RSVP keyboard: An EEG based typing interface. In *2012 IEEE International Conference on Acoustics, Speech and Signal Processing (ICASSP)*, pages 645–648. IEEE, 2012.

[24] Ary L Goldberger, Luis AN Amaral, Leon Glass, Jeffrey M Hausdorff, Plamen Ch Ivanov, Roger G Mark, Joseph E Mietus, George B Moody, Chung-Kang Peng, and H Eugene Stanley. Physiobank, physiotoolkit, and physionet: components of a new research resource for complex physiologic signals. *circulation*, 101(23):e215–e220, 2000.

[25] Perrin Margaux, Maby Emmanuel, Daligault Sébastien, Bertrand Olivier, and Mattout Jérémie. Objective and subjective evaluation of online error correction during P300-based spelling. *Advances in Human-Computer Interaction*, 2012, 2012.

[26] Justin Bayer, Daan Wierstra, Julian Togelius, and Jürgen Schmidhuber. Evolving memory cell structures for sequence learning. In *International Conference on Artificial Neural Networks*, pages 755–764. Springer, 2009.

[27] Rafal Jozefowicz, Wojciech Zaremba, and Ilya Sutskever. An empirical exploration of recurrent network architectures. In *International conference on machine learning*, pages 2342–2350, 2015.

[28] Ekin D Cubuk, Barret Zoph, Dandelion Mane, Vijay Vasudevan, and Quoc V Le. AutoAugment: Learning augmentation strategies from data. In *Proceedings of the IEEE conference on computer vision and pattern recognition*, pages 113–123, 2019.

[29] Daniel S Park, William Chan, Yu Zhang, Chung-Cheng Chiu, Barret Zoph, Ekin D Cubuk, and Quoc V Le. SpecAugment: A simple data augmentation method for automatic speech recognition. *arXiv preprint arXiv:1904.08779*, 2019.

[30] Diederik P Kingma and Max Welling. Auto-encoding variational Bayes. *arXiv preprint arXiv:1312.6114*, 2013.

[31] Ian Goodfellow, Jean Pouget-Abadie, Mehdi Mirza, Bing Xu, David Warde-Farley, Sherjil Ozair, Aaron Courville, and Yoshua Bengio. Generative adversarial nets. In *Advances in neural information processing systems*, pages 2672–2680, 2014.

[32] Vincent Dumoulin, Ishmael Belghazi, Ben Poole, Olivier Mastropietro, Alex Lamb, Martin Arjovsky, and Aaron Courville. Adversarially learned inference. *arXiv preprint arXiv:1606.00704*, 2016.

[33] Jeff Donahue, Philipp Krähenbühl, and Trevor Darrell. Adversarial feature learning. *arXiv preprint arXiv:1605.09782*, 2016.

[34] Eric Jang, Shixiang Gu, and Ben Poole. Categorical reparameterization with Gumbel-softmax. *arXiv preprint arXiv:1611.01144*, 2016.

[35] Kai J Miller, Dora Hermes, Nathan Witthoft, Rajesh PN Rao, and Jeffrey G Ojemann. The physiology of perception in human temporal lobe is specialized for contextual novelty. *Journal of neurophysiology*, 114(1):256–263, 2015.

[36] Kai J Miller, Gerwin Schalk, Dora Hermes, Jeffrey G Ojemann, and Rajesh PN Rao. Spontaneous decoding of the timing and content of human object perception from cortical surface recordings reveals complementary information in the event-related potential and broadband spectral change. *PLoS computational biology*, 12(1), 2016.

[37] Kai J Miller, Dora Hermes, Franco Pestilli, Gagan S Wig, and Jeffrey G Ojemann. Face percept formation in human ventral temporal cortex. *Journal of neurophysiology*, 118(5):2614–2627, 2017.

[38] Stefano Pizzolato, Luca Tagliapietra, Matteo Cognolato, Monica Reggiani, Henning Müller, and Manfredo Atzori. Comparison of six electromyography acquisition setups on hand movement classification tasks. *PloS one*, 12(10), 2017.

## Appendix

### A.1 Related Work

This paper relates some existing literature as follows.

- **AutoML:** Searching DNN models with hyperparameter optimization has been intensively investigated in a related framework called AutoML [11–19]. The automated methods include architecture search [14, 16, 17, 19], learning rule design [26, 27], and augmentation exploration [28, 29]. Most work used either evolutionary optimization or reinforcement learning framework to adjust hyperparameters or to construct network architecture from pre-selected building blocks. Recent AutoML-Zero [17] considers an extension to preclude human knowledge and insights for fully automated designs from scratch.
- **Variational Bayesian Inference:** The VAE [30] introduced variational Bayesian inference methods, incorporating autoassociative architectures, where generative and inference models can be learned jointly. This method was extended with the CVAE [10], which introduces a conditioning variable that could be used to represent nuisance variations, and a regularized VAE in [9], which considers disentangling the nuisance variable from the latent representation.
- **Adversarial Training:** The concept of adversarial was introduced with Generative Adversarial Networks (GAN) [31], and has been adopted into myriad applications. The simultaneously discovered Adversarially Learned Inference (ALI) [32] and Bidirectional GAN (BiGAN) [33] propose an adversarial approach toward training an autoencoder. Adversarial training has also been combined with VAE to regularize and/or disentangle the latent representations [6–8].

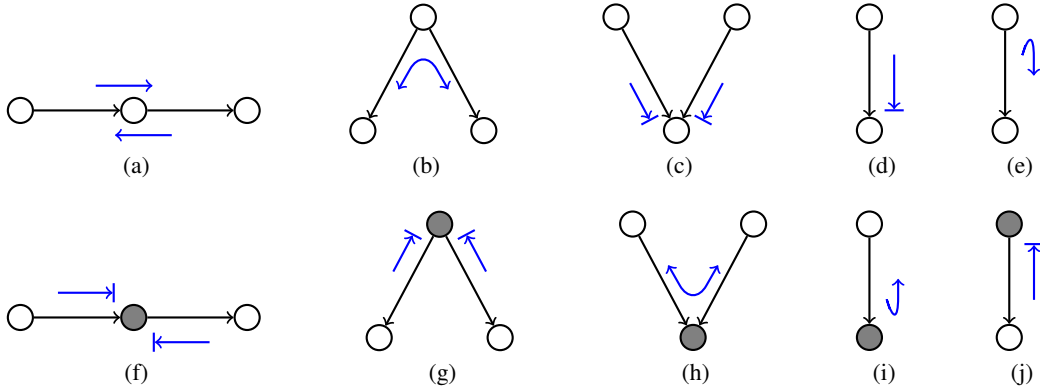


Figure 6: Bayes-Ball algorithm basic rules [20]. Conditional nodes are shaded.

The main contributions of this paper over the existing works is five-fold as follows:

- AutoBayes explores potential graphical models inherent to the data, rather than exploring hyperparameters of DNN blocks.
- AutoBayes offers a solid reason of how to connect multiple DNN blocks to impose conditioning and adversary censoring for the task classifier, feature encoder, decoder, nuisance indicator and adversary networks, based on an explored Bayesian graph.
- It provides a systematic automation framework to explore different inference models through the use of the Bayes-Ball algorithm and ordered factorization.
- The framework is also extensible to multiple latent representations and multiple nuisances factors.
- Besides fully-supervised training, AutoBayes can automatically build some relevant graphical models suited for semi-supervised learning.

## A.2 Bayes-Ball Algorithm

The Bayes-Ball algorithm [20] facilitates an automatic pruning of links in inference factor graphs through the analysis of conditional independency. The algorithm uses ten rules to identify conditional independency as shown in Fig. 6. Given directed Bayesian graphs, we can determine whether a conditional independence between two disjoint sets of nodes given conditioning on other nodes by applying a graph separation criterion. Specifically, an undirected path is activated if a Bayes ball can travel along without encountering a stop symbol:  $\rightarrow$  in Fig. 6. If there are no active paths between two sets of nodes when some other conditioning nodes are shaded, then those sets of random variables are conditionally independent.

## A.3 AutoBayes Algorithm

The overall procedure of the AutoBayes algorithm is described in the pseudocode of Algorithm 1. The AutoBayes automatically constructs non-redundant inference factor graphs given a hypothetical Bayesian graph assumption, through the use of the Bayes-Ball algorithm. Depending on the derived conditional independency and pruned factor graphs, DNN blocks for encoder  $\mathcal{E}$ , decoder  $\mathcal{D}$ , classifier  $\mathcal{C}$ , nuisance estimator  $\mathcal{N}$  and adversary  $\mathcal{A}$  are reasonably connected. The whole DNN blocks are trained with adversary learning in a variational Bayesian inference. Note that hyperparameters of each DNN block can be further optimized by AutoML on top of AutoBayes framework.

## A.4 Variational Bayesian Inference with Adversarial Training

**Variational AE** AutoBayes may automatically construct autoencoder architecture when latent variables are involved, e.g., for the model E in Fig. 3(e). For this case,  $Z$  represents a stochastic node to marginalize out for  $X$  reconstruction and  $Y$  inference, and hence VAE will be required. In

---

**Algorithm 1** Pseudocode for AutoBayes Framework

---

**Require:** Nodes set  $\mathcal{V} = [Y, X, S_1, S_2, \dots, S_n, Z_1, Z_2, \dots, Z_m]$ , where  $Y$  denotes task labels,  $X$  is a measurement data,  $\mathcal{S} = [S_1, S_2, \dots, S_n]$  are (potentially multiple) semi-supervised nuisance variations, and  $\mathcal{Z} = [Z_1, Z_2, \dots, Z_m]$  are (potentially multiple) latent vectors

**Ensure:** Semi-supervised training/validation datasets

- 1: **for all** permutations of node factorization from  $Y$  to  $X$  **do**
- 2:     Let  $\mathcal{B}_0$  be the corresponding Bayesian graph for the permuted full-chain factorization  $p(y) \cdots p(z_1 | \dots) \cdots p(x | \dots)$
- 3:     **for all** combinations of link pruning on the full-chain Bayesian graph  $\mathcal{B}_0$  **do**
- 4:         Let  $\mathcal{B}$  be the corresponding pruned Bayesian graph
- 5:         Apply the Bayes-Ball algorithm on  $\mathcal{B}$  to build a conditional independency list  $\mathcal{I}$
- 6:         **for all** permutations of node factorization from  $X$  to  $Y$  **do**
- 7:             Let  $\mathcal{F}_0$  be the corresponding factor graph, representing a full-chain conditional probability  $p(\cdot | x) \cdots p(z_1 | \dots) \cdots p(y | \dots, x)$
- 8:             Prune all redundant links in  $\mathcal{F}_0$  based on conditional independency  $\mathcal{I}$
- 9:             Let  $\mathcal{F}$  be the pruned factor graph
- 10:             Merge the pruned Bayesian graph  $\mathcal{B}$  into the pruned factor graph  $\mathcal{F}$
- 11:             Attach an adversary network  $\mathcal{A}$  to latent nodes  $\mathcal{Z}$  for  $Z_k \perp \mathcal{S} \in \mathcal{I}$
- 12:             Assign an encoder network  $\mathcal{E}$  for  $p(\mathcal{Z} | \dots)$  in the merged factor graph
- 13:             Assign a decoder network  $\mathcal{D}$  for  $p(x | \dots)$  in the merged factor graph
- 14:             Assign a nuisance indicator network  $\mathcal{N}$  for  $p(\mathcal{S} | \dots)$  in the merged factor graph
- 15:             Assign a classifier network  $\mathcal{C}$  for  $p(y | \dots)$  in the merged factor graph
- 16:             Adversary train the whole DNN structure with variational reparameterization to minimize a loss function in (11)
- 17:         **end for** ▷ At most  $(|\mathcal{V}| - 2)!$  combinations
- 18:     **end for** ▷ At most  $2^{|\mathcal{V}|(|\mathcal{V}| - 1)/2}$  combinations
- 19: **end for** ▷ At most  $(|\mathcal{V}| - 2)!$  combinations
- 20: **return** the best model having highest task accuracy in validation sets

---

contrast to vanilla autoencoders, VAE uses variational inference by assuming a marginal distribution for latent  $p(z)$ . In variational approach, we reparameterize  $Z$  from a prior distribution such as the normal distribution to marginalize. Depending on the Bayesian graph models, we can also consider reparameterizing semi-supervision on  $S$  (i.e., incorporating a reconstruction loss for  $S$ ) as a conditioning variable. Conditioning on  $Y$  and/or  $S$  should depend on consistency with the graphical model assumptions. Since VAE is a special case of CVAE, we will go into further detail about the more general CVAE below.

**Conditional VAE** When  $X$  is directly dependent on  $S$  or  $Y$  along with  $Z$  in the Bayesian graph, the AutoBayes gives rise the CVAE architecture, e.g., for the models E/F/G/H/I in Fig. 3. For those generative models, the decoder DNN needs to feed  $S$  or  $Y$  as a conditioning parameter. Even for other Bayesian graphs, the  $S$ -first inference strategy will require conditional encoder in CVAE, e.g., the models Ds/Es/Fs/Gs/Js/Ks in Fig. 4, where latent  $Z$  depends on  $S$ .

Consider the case when  $S$  plays as the conditioning variable in a data model with the factorization:

$$p(s, x, z) = p(s)p(z)p(x|s, z), \quad (13)$$

where we directly parameterize  $p(x|s, z)$ , set  $p(z)$  to something simple (e.g., isotropic Gaussian), and leave  $p(s)$  arbitrary (since it will not be directly used). The CVAE is trained according to maximizing the likelihood of data tuples  $(s, x)$  with respect to  $p(x|s)$ , which is given by

$$p(x|s) = \int p(x|s, z)p(z) dz, \quad (14)$$

which is intractable to compute exactly given the potential complexity of the parameterization of  $p(x|s, z)$ . While it could be possible to approximate the integration with sampling of  $Z$ , the crux of the VAE approach is to utilize a variational lower-bound of the likelihood that involves a variational approximation of the posterior  $p(z|s, x)$  implied by the generative model. With  $q(z|s, x)$  representing the variational approximation of the posterior, the Evidence Lower-Bound (ELBO) is

given by

$$\log p(x|s) \geq \mathbb{E}_{z \sim q(z|s,x)}[\log p(x|s,z)] - \mathbb{KL}(q(z|s,x)\|p(z)). \quad (15)$$

The parameterization of the variational posterior  $q(z|s,x)$  may also be decomposed into parameterized components, e.g.,  $q(z|s,x) = q(s|x)q(z|s,x)$  such as in the  $S$ -first models shown in Fig. 4. Such decomposition also enables the possibility of semi-supervised training, which can be convenient when some of the variables, such as the nuisances variations, are not always labeled. For data tuples that include  $s$ , the likelihood  $q(s|x)$  can also be directly optimized, and the given value for  $s$  is used an input to the computation of  $q(z|s,x)$ . However, for tuples where  $s$  is missing, the component  $q(s|x)$  can be used to generate an estimate of  $s$  to be input to  $q(z|s,x)$ . We further discuss semi-supervised learning and the sampling methods for categorical nuisance variables in Appendix A.5 below.

**Adversarial CVAE** We can utilize adversary censoring when  $Z$  and  $S$  should be marginally independent, e.g., such as in Fig. 1(b) and Fig. 5, in order to reinforce the learning of a representation  $Z$  that is disentangled from the nuisance variations  $S$ . This is accomplished by introducing an adversarial network that aims to maximize a parameterized approximation  $q(s|z)$  of the likelihood  $p(s|z)$ , while this likelihood is also incorporated into the loss for the other modules with a negative weight. The adversarial network, by maximizing the log likelihood  $\log q(s|z)$ , essentially maximizes a lower-bound of the mutual information  $\mathbb{I}(S;Z)$ , and hence the main network is regularized with the additional term that corresponds to minimizing this estimate of mutual information. This follows since the log-likelihood maximized by the adversarial network is given by

$$\mathbb{E}[\log q(s|z)] = \mathbb{I}(S;Z) - \mathbb{H}(S) - \mathbb{KL}(p(s|z)\|q(s|z)), \quad (16)$$

where the entropy  $\mathbb{H}(S)$  is constant.

## A.5 Semi-Supervised Learning: Categorical Sampling

**Graphical Models for Semi-Supervised Learning** Nuisance values  $S$  such as subject ID or session ID may not be always available for typical physiological datasets, in particular for the testing phase of an HMI system deployment with new users, requiring semi-supervised methods. We note that some graphical models are well-suited for such semi-supervised training. For example, among the Bayesian graph models in Fig. 3, the models C/E/G/I require the nuisance  $S$  to reproduce  $X$ . If no ground-truth labels of  $S$  are available, we need to marginalize  $S$  across all possible categories for the decoder DNN  $\mathcal{D}$ . Even for other Bayesian graphs, the corresponding inference factor graphs in Fig. 4 may not be convenient for the semi-supervised settings. Specifically, for models Ez/Fz/Jz/Kz have an inference of  $S$  at the end node, whereas the other inference models use inferred  $S$  for subsequent inference of other parameters. If  $S$  is missing or unknown as a semi-supervised setting, those inference graphs having  $S$  in a middle node are inconvenient as we need sampling over all possible nuisance categories. For instance, the model Kz shown in Fig. 5 does not need  $S$  marginalization, and thus readily applicable to semi-supervised datasets.

**Variational Categorical Reparameterization** In order to deal with the issue of categorical sampling, we can use the Gumbel-Softmax reparameterization trick [34], which enables differentiable approximation of one-hot encoding. Let  $[\pi_1, \pi_2, \dots, \pi_{|S|}]$  denote a target probability mass function for the categorical variable  $S$ . Let  $g_1, g_2, \dots, g_{|S|}$  be independent and identically distributed samples drawn from the Gumbel distribution  $\text{Gumbel}(0, 1)$ .<sup>1</sup> Then, generate an  $|S|$ -dimensional vector  $\hat{s} = [\hat{s}_1, \hat{s}_2, \dots, \hat{s}_{|S|}]$  according to

$$\hat{s}_k = \frac{\exp((\log(\pi_k) + g_k)/\tau)}{\sum_{i=1}^{|S|} \exp((\log(\pi_i) + g_i)/\tau)}, \quad (17)$$

where  $\tau > 0$  is a softmax temperature. As the softmax temperature  $\tau$  approaches 0, samples from the Gumbel-Softmax distribution become one-hot and the distribution becomes identical to the target categorical distribution. The temperature  $\tau$  is usually decreased across training epochs as an annealing technique, e.g., with exponential decaying.

<sup>1</sup>The Gumbel(0, 1) distribution can be sampled using inverse transform sampling by drawing  $u \sim \text{Uniform}(0, 1)$  and computing  $g = -\log(-\log(u))$ .

Table 2: Dataset parameters

Datasets	Modality	Dimension	Nuisance ( $ S $ )	Labels ( $ Y $ )	Samples
QMNST Stress RSVP MI ErrP	Image	$28 \times 28$	539	10	60,000
	Temperature etc.	7	20	4	24,000
	EEG	$16 \times 128$	10	4	41,400
	EEG	$64 \times 480$	106	4	9,540
	EEG	$56 \times 250$	27	2	9,180
Faces Basic	ECoG	$31 \times 400$	14	2	4,100
Faces Noisy	ECoG	$39 \times 400$	7	2	2,100
Ninapro	EMG	16	10	12	890,446

## A.6 Datasets Description

We used publicly available physiological datasets as well as a benchmark MNIST as follows. The parameters of datasets are also summarized in Table 2.

- **QMNST:** A hand-written digit image MNIST with extended label information including a writer ID number [21].<sup>2</sup> There are  $|S| = 539$  writers for classifying  $|Y| = 10$  digits from grayscale  $28 \times 28$  pixel images over 60,000 training samples. Another 535 writers provide 60,000 test samples.
- **Stress:** A physiological dataset considering neurological stress level [22].<sup>3</sup> It consists of multi-modal biosignals for  $|Y| = 4$  discrete stress states from  $|S| = 20$  healthy subjects, including physical/cognitive/emotional stresses as well as relaxation. The data were collected by  $C = 7$  sensors, i.e., electrodermal activity, temperature, three-dimensional acceleration, heart rate, and arterial oxygen level. For each stress status, a corresponding task of 5 minutes long (i.e.,  $T = 300$  time samples with 1 Hz down-sampling) was assigned to subjects for a total of 4 trials.
- **RSVP:** An EEG-based typing interface using rapid serial visual presentation (RSVP) paradigm [23].<sup>4</sup>  $|S| = 10$  healthy subjects participated in the experiments at three sessions performed on different days. The dataset consists of 41,400 epochs of  $C = 16$  channel EEG data for  $T = 128$  samples, which were collected by g.USBamp biosignal amplifier with active electrodes during RSVP keyboard operations.  $|Y| = 4$  labels for emotion elicitation, resting-state, or motor imagery/execution task.
- **MI:** The PhysioNet EEG Motor Imagery (MI) dataset [24].<sup>5</sup> Excluding irregular timestamp, the dataset consists of  $|S| = 106$  subjects' EEG data. During the experiments, subjects were instructed to perform cue-based motor execution/imagery tasks while  $C = 64$  channels were recorded at a sampling rate of 160 Hz. Focusing on motor imagery tasks, we use the EEG data for three seconds of post-cue interval data (i.e.,  $T = 480$  time samples). The subject performed  $|Y| = 4$ -class tasks; either right hand motor imagery, left hand motor imagery, both hands motor imagery, or both feet motor imagery. This resulted in a total of 90 trials per subject.
- **ErrP:** An error-related potential (ErrP) of front-central EEG dataset [25].<sup>6</sup> The dataset consists of EEG data recorded from  $|S| = 16$  healthy subjects participating in an offline P300 spelling task, where visual feedback of the inferred letter is provided to the user at the end of each trial for 1.3 seconds to monitor evoked brain responses for erroneous decisions made by the system. EEG data were recorded from  $C = 56$  channels for epoched 1.25 seconds at a sampling rate of 200 Hz (i.e.,  $T = 250$ ). Across five recording sessions, each subject performed a total of 340 trials. Since it was an offline copy spell task, binary  $|Y| = 2$  labels were provided as erroneous or correct feedback.

<sup>2</sup>QMNST dataset: <https://github.com/facebookresearch/qmnist>

<sup>3</sup>Stress dataset: <https://physionet.org/content/noneeg/1.0.0/>

<sup>4</sup>RSVP dataset: <http://hdl.handle.net/2047/D20294523>

<sup>5</sup>MI dataset: <https://physionet.org/physiobank/database/eegmmidb/>

<sup>6</sup>ErrP dataset: <https://www.kaggle.com/c/inria-bci-challenge/>

- **Faces Basic:** An implanted electrocorticography (ECoG) array dataset for visual stimulus experiments [35, 36].<sup>7</sup> ECoG arrays were implanted on the subtemporal cortical surface of  $|S| = 7$  epilepsy patients.  $|Y| = 2$  classes of grayscale images, either faces or houses, were displayed rapidly in random sequence for 400 ms each with black-screen intervals of 400 ms. The ECoG potentials were measured with respect to a scalp reference and ground, at a sampling rate of 1000 Hz. Subjects performed a basic face and house discrimination task. There were 3 sessions for each patient, with 50 house pictures and 50 face pictures in each run, in total 4,100 samples. We use the first  $C = 31$  channels to analyze for  $T = 400$ . Reusing the public dataset requires the ethics statement information.<sup>8</sup>
- **Faces Noisy:** The implanted ECoG arrays dataset for visual stimulus experiments [35, 37]. The experiment is similar to Faces Basic dataset, while pictures of faces and houses are randomly scrambled. Refer ethics statement to reuse the dataset.<sup>9</sup>
- **Ninapro:** An EMG dataset for fingers motion detection for prosthetic hands [38].<sup>10</sup> The subjects repeated several finger movements represented by movies that are shown on the screen of a laptop. Each movement repetition lasted 5 seconds and was followed by 3 seconds of rest. The dataset includes 6 trials of  $|Y| = 12$  different movements (plus rest) performed by  $|S| = 10$  intact subjects. The muscular activity was gathered using two Thalmic Myo armbands, having  $C = 16$  active differential wireless electrodes. The EMG signals are sampled at a rate of 200 Hz.

The additional results for the supplemental datasets using the ECoG and EMG modalities are listed in Table 3.

### A.7 DNN Model Parameters

For 2D datasets, we use deep CNN for the encoder  $\mathcal{E}$  and decoder  $\mathcal{D}$  blocks. For the classifier  $\mathcal{C}$ , nuisance estimator  $\mathcal{N}$ , and adversary  $\mathcal{A}$ , we use a multi-layer perceptron (MLP) having three layers, whose hidden nodes are doubled from the input dimension. We also use batch normalization (BN) and ReLU activation as listed in Table 4. Note that for a tabular data such as Stress datasets, CNN was replaced with 3-layer MLP having ReLU activation and dropout with a ratio of 20%. Also the MLP classifier was replaced with CNN for 2D input dimension cases such as in the model A. The number of latent dimensions was chosen  $|Z| = 64$ . When we need to feed  $S$  along with 2D data of  $X$  into the CNN encoder such as in the model Ds, we use an interpolation to concatenate as additional channel input. We use  $\lambda_* = 0.01$  for the regularization coefficient. We leave hyperparameter exploration to integrate AutoML and AutoBayes as a remaining future work.

---

<sup>7</sup>Faces dataset: <https://exhibits.stanford.edu/data/catalog/zk881ps0522>

<sup>8</sup> **Ethics statement:** All patients participated in a purely voluntary manner, after providing informed written consent, under experimental protocols approved by the Institutional Review Board of the University of Washington (#12193). All patient data was anonymized according to IRB protocol, in accordance with HIPAA mandate. These data originally appeared in the manuscript “Spontaneous Decoding of the Timing and Content of Human Object Perception from Cortical Surface Recordings Reveals Complementary Information in the Event-Related Potential and Broadband Spectral Change” published in PLoS Computational Biology in 2016 [36].

<sup>9</sup> All patients participated in a purely voluntary manner, after providing informed written consent, under experimental protocols approved by the Institutional Review Board of the University of Washington (#12193). All patient data was anonymized according to IRB protocol, in accordance with HIPAA mandate. These data originally appeared in the manuscript “Face percept formation in human ventral temporal cortex” published in Journal of Neurophysiology in 2017 [37].

<sup>10</sup>Ninapro dataset: <https://zenodo.org/record/1000116#.XuIppS2z30R>

Table 3: Performance of additional datasets: the reconstruction loss, the scores of nuisance classification and task classification in variational/non-variational and adversarial/non-adversarial setting.

Dataset	Method	Reconstruction Loss (dB)		Nuisance Classification (%)		Task Classification (%)	
		Non-Variational	Variational	Non-Variational	Variational	Non-Variational	Variational
Faces Basic	Model A	-32.5	—	—	—	61.2	—
	Model B	-39.2	-31.7	—	—	51.0	52.1
	Model Cs	-34.6	—	97.1	—	61.6	—
	Model Cy	-34.8	—	97.0	—	<b>68.1</b>	—
	Model Ds	-39.4	-32.5	98.5	96.0	63.9	63.7
	Model Dz	-39.1	-35.7	34.2	7.6	51.5	53.2
	Model Es	-39.3	-34.3	98.0	98.5	51.5	51.9
	Model Ez	-39.3	<b>-35.8</b>	97.8	96.9	50.6	51.1
	Model Fs	-39.3	-32.3	97.2	98.2	64.9	63.2
	Model Fz	-39.3	-33.5	<b>28.4</b>	6.3	63.7	62.2
	Model Gs	-39.3	-34.5	96.8	97.0	51.3	<b>49.7</b>
	Model Gz	-39.4	-33.3	98.1	97.7	51.0	52.5
	Model H	<b>-42.5</b>	-32.9	98.1	96.4	62.2	62.0
	Model I	-39.3	-33.3	97.6	98.7	60.6	<b>68.1</b>
	Model Js	-40.8	-34.3	98.0	98.1	51.1	51.2
	Model Jz	-40.5	-34.0	42.3	33.1	51.5	52.3
	Model Ks	-40.8	-33.7	97.7	98.2	<b>49.4</b>	52.3
	Model Kz	-40.4	-30.1	33.2	<b>5.8</b>	51.6	50.6
Faces Noisy	Model A	-32.3	—	—	—	73.8	—
	Model B	-35.9	-22.5	—	—	49.5	50.3
	Model Cs	-32.1	—	95.8	—	74.4	—
	Model Cy	-31.9	—	98.3	—	68.1	—
	Model Ds	-35.2	-31.8	97.7	96.6	71.1	71.3
	Model Dz	-35.7	-22.4	<b>33.4</b>	14.2	50.2	52.5
	Model Es	-35.7	-32.6	96.3	98.0	50.5	53.1
	Model Ez	-35.8	-19.1	98.4	97.8	50.3	51.5
	Model Fs	-35.7	-32.8	97.1	98.2	64.9	63.2
	Model Fz	-35.6	-21.3	39.2	<b>12.0</b>	75.5	67.2
	Model Gs	-35.8	-32.2	96.4	97.0	50.3	50.5
	Model Gz	-35.6	-25.1	98.0	98.0	<b>49.2</b>	51.3
	Model H	-35.9	-27.7	97.0	96.3	73.4	<b>73.4</b>
	Model I	-34.6	-26.1	97.7	97.5	<b>76.7</b>	73.0
	Model Js	<b>-39.3</b>	-36.2	98.3	98.4	51.9	50.8
	Model Jz	-37.7	-30.0	33.6	13.1	50.8	<b>50.2</b>
	Model Ks	<b>-39.3</b>	<b>-37.1</b>	98.9	98.8	50.9	53.0
	Model Kz	-37.4	-30.0	34.8	12.2	52.8	50.5

Table 3: Performance of additional datasets (continued)

Dataset	Method	Reconstruction Loss (dB)		Nuisance Classification (%)		Task Classification (%)	
		Non-Variational	Variational	Non-Variational	Variational	Non-Variational	Variational
Ninapro	Model A	-37.2	—	—	—	<b>69.9</b>	—
	Model B	-51.4	-36.1	—	—	65.3	62.0
	Model Cs	-37.8	—	45.3	—	67.7	—
	Model Cy	-37.8	—	44.6	—	67.9	—
	Model Ds	-52.1	-36.1	45.5	45.5	67.4	<b>68.9</b>
	Model Dz	-51.6	-36.1	<b>21.8</b>	<b>10.2</b>	65.4	63.0
	Model Es	-50.8	-36.5	45.5	45.1	65.1	62.0
	Model Ez	-51.2	-36.1	45.7	44.3	65.5	62.1
	Model Fs	-51.3	-36.1	45.6	45.4	68.5	67.5
	Model Fz	<b>-57.9</b>	-41.0	22.9	21.6	64.8	62.0
	Model Gs	-51.0	-36.5	45.4	44.1	66.9	63.4
	Model Gz	-51.5	-36.1	45.5	44.1	66.2	63.6
	Model H	-51.0	-36.1	45.6	44.1	67.2	66.6
	Model I	-51.5	-36.1	45.5	44.5	69.0	66.5
	Model Js	-58.4	<b>-42.0</b>	45.4	45.3	63.4	65.1
	Model Jz	-37.7	-30.0	33.6	13.1	<b>50.8</b>	<b>50.2</b>
	Model Ks	<b>-57.9</b>	-36.7	45.7	45.3	66.1	64.1
	Model Kz	-58.1	-41.1	22.3	21.2	68.9	65.9

Table 4: DNN model parameters in Fig. 5;  $\text{Conv}(h, w)_g^c$  denotes 2D convolution layer with kernel size of  $(h, w)$  for output channel of  $c$  over group  $g$ .  $\text{FC}(h)$  denotes fully-connected layer with  $h$  output nodes. BN denotes batch normalization.

Classifier $\mathcal{C}$	Encoder $\mathcal{E}$	Decoder $\mathcal{D}$	Nuisance $\mathcal{N}$	Adversary $\mathcal{A}$
$\text{FC}(2 Z )$	$\text{Conv}(1, 15)^{50}$	$\text{FC}(20T)$	$\text{FC}(2 Z )$	$\text{FC}(2 Z )$
BN+ReLU	BN+ReLU	ReLU	BN+ReLU	BN+ReLU
$\text{FC}( Y )$	$\text{Conv}(1, 7)^{50}$ BN+ReLU	$\text{Conv}(C, 1)^{50}$ BN+ReLU	$\text{FC}( S )$	$\text{FC}( S )$
	$\text{Conv}(1, 3)^{50}$ BN+ReLU	$\text{Conv}(1, 3)^{50}$ BN+ReLU		
	$\text{Conv}(C, 1)^{50}$	$\text{Conv}(1, 7)^{50}$		
	$\text{FC}( Z )$	BN+ReLU		
		$\text{Conv}(1, 15)^{50}$		